Original Article | Gastrointestinal Imaging

eISSN 2005-8330
https://doi.org/10.3348/kjr.2021.0407
Korean J Radiol 2022;23(4):389-401

Korean Journal of Radiology
KJR

Total Bilirubin Level as a Predictor of Suboptimal Image Quality of the Hepatobiliary Phase of Gadoxetic Acid-Enhanced MRI in Patients with Extrahepatic Bile Duct Cancer

Jeong Ah Hwang[1], Ji Hye Min[1], Seong Hyun Kim[1], Seo-Youn Choi[2], Ji Eun Lee[2], Ji Yoon Moon[3]

[1]Department of Radiology and Center for Imaging Science, Samsung Medical Center, Sungkyunkwan University School of Medicine, Seoul, Korea; [2]Department of Radiology, Soonchunhyang University Bucheon Hospital, Soonchunhyang University College of Medicine, Bucheon, Korea; [3]Department of Radiology, Kangdong Seong-Sim Hospital, Hallym University College of Medicine, Seoul, Korea

Objective: This study aimed to determine a factor for predicting suboptimal image quality of the hepatobiliary phase (HBP) of gadoxetic acid-enhanced MRI in patients with extrahepatic bile duct (EHD) cancer before MRI examination.

Materials and Methods: We retrospectively evaluated 259 patients (mean age ± standard deviation: 68.0 ± 8.3 years; 162 male and 97 female) with EHD cancer who underwent gadoxetic acid-enhanced MRI between 2011 and 2017. Patients were divided into a primary analysis set (n = 184) and a validation set (n = 75) based on the diagnosis date of January 2014. Two reviewers assigned the functional liver imaging score (FLIS) to reflect the HBP image quality. The FLIS consists of the sum of three HBP features, each scored on a 0–2 scale: liver parenchymal enhancement, biliary excretion, and signal intensity of the portal vein. Patients were classified into low-FLIS (0–3) or high-FLIS (4–6) groups. Multivariable analysis was performed to determine a predictor of low FLIS using serum biochemical and imaging parameters of cholestasis severity. The optimal cutoff value for predicting low FLIS was obtained using receiver operating characteristic analysis, and validation was performed.

Results: Of the 259 patients, 140 (54.0%) and 119 (46.0%) were classified into the low-FLIS and high-FLIS groups, respectively. In the primary analysis set, total bilirubin was an independent factor associated with low FLIS (adjusted odds ratio per 1-mg/dL increase, 1.62; 95% confidence interval [CI], 1.32–1.98). The optimal cutoff value of total bilirubin for predicting low FLIS was 2.1 mg/dL with a sensitivity of 95.1% (95% CI: 88.9–98.4) and a specificity of 89.0% (95% CI: 80.2–94.9). In the validation set, the total bilirubin cutoff showed a sensitivity of 92.1% (95% CI: 78.6–98.3) and a specificity of 83.8% (95% CI: 68.0–93.8).

Conclusion: Serum total bilirubin before acquisition of gadoxetic acid-enhanced MRI may help predict suboptimal HBP image quality in patients with EHD cancer.

Keywords: *Hyperbilirubinemia; Cholestasis; Gadolinium DTPA; Magnetic resonance imaging; Bile duct neoplasms*

INTRODUCTION

Gadolinium ethoxybenzyl diethylenetriamine pentaacetic acid (Gd-EOB-DTPA, gadoxetic acid; Eovist or Primovist; Bayer HealthCare) provides excellent lesion-to-liver contrast during the hepatobiliary phase (HBP). This is because approximately 50% of Gd-EOB-DTPA is taken up into the functional hepatocytes, and intense hepatic parenchymal enhancement is obtained 20 minutes after contrast administration [1,2]. In patients with biliary obstructions such as extrahepatic bile duct (EHD) cancer, however, the hepatocyte uptake of Gd-EOB-DTPA and its biliary excretion

Received: March 3, 2021 **Revised:** October 16, 2021 **Accepted:** October 30, 2021
Corresponding author: Ji Hye Min, MD, PhD, Department of Radiology and Center for Imaging Science, Samsung Medical Center, Sungkyunkwan University School of Medicine, 81 Irwon-ro, Gangnam-gu, Seoul 06351, Korea.
• E-mail: minjh1123@gmail.com

can be reduced, because Gd-EOB-DTPA uptake is mediated by the same transporter responsible for bilirubin transport [3].

CT and MRI with MR cholangiopancreatography (MRCP) are widely used for the preoperative staging of EHD cancer. There have been only a few studies on the applications of gadoxetic acid-enhanced MRI for EHD cancer [4,5], and no consensus has been reached on which MRI contrast agent can be used to evaluate EHD cancer. Despite several drawbacks such as transient motion artifacts [6] and weak vascular enhancement caused by lower amounts of Gd-EOB-DTPA [7], the reason for implementing gadoxetic acid-enhanced MRI in patients with EHD cancer may be the high sensitivity of the HBP images for the detection of focal liver lesions, particularly sub-centimeter lesions [8,9]. A previous study reported the usefulness of gadoxetic acid-enhanced MRI for distinguishing hepatic micro-abscesses due to biliary obstruction from metastases [10]. Because inflammatory lesions appear smaller on unenhanced T1-weighted images than on HBP images, a significant size discrepancy suggests a micro-abscess rather than a metastasis [10]. Therefore, it is important to obtain adequate hepatic parenchymal enhancement on HBP images in patients with EHD cancer.

To our knowledge, only a few studies have evaluated the relationship between liver function parameters and the HBP image quality of gadoxetic acid-enhanced MRI [3,11,12]. These studies included patients with various diseases, including chronic liver disease or pancreaticobiliary cancer, and were evaluated without quantitative or simple parameters reflecting the HBP image quality. The functional liver imaging score (FLIS) is a semi-quantitative scoring system that reflects the HBP image quality because it is derived from the three HBP features of gadoxetic acid-enhanced MRI [13,14]. Predicting low FLIS before MRI examination may help in selecting the optimal MR contrast agent. Therefore, the purpose of this study was to determine the factors associated with suboptimal HBP image quality among the serum biochemical and imaging parameters of biliary obstruction, using the FLIS from the HBP features of gadoxetic acid-enhanced MRI in patients with EHD cancer.

MATERIALS AND METHODS

This retrospective study was approved by the Institutional Review Board of Samsung Medical Center (IRB No. SMC 2020-12-062), and the requirement for informed consent was waived.

Patients

A total of 1864 consecutive patients who had pathologically confirmed EHD cancer by surgery or biopsy between January 2011 and September 2017 were identified through a search of our institution's registry. In accordance with the following criteria, 290 patients were included: 1) patients with distal common bile duct cancer or Bismuth classification I perihilar cancer, 2) patients who underwent gadoxetic acid-enhanced MRI obtained within three months before surgery or biopsy, 3) available preoperative laboratory results within two days of the MRI, and 4) contrast-enhanced CT obtained within 2 weeks before the MRI. Thirty-one patients were excluded according to the following criteria: 1) ten patients with markedly degraded MRI image quality due to artifacts, and 21 patients without follow-up CT/MRI for at least 6 months. We measured the diameter of the dilated upstream common duct to determine its role as an imaging predictor; therefore, among perihilar cancers, only Bismuth classification I cancers were included. Finally, 259 patients were included in the study. Patients were divided into two groups based on the date of EHD cancer diagnosis on January 1, 2014, and patients after the date were allocated into the primary analysis set and those before the date were allocated into the validation set (Fig. 1).

CT and MRI Acquisition

CT scans were performed using one of the following multidetector CT scanners: Somatom Definition Flash 128 (Siemens Healthineers), Toshiba Aquilion 64 detector (Toshiba Medical Systems), and LightSpeed VCT 64 or Discovery CT 750 (GE Healthcare). MRI was performed using a 3T MR system (Achieva 3T, Philips Healthcare). MRI included unenhanced T1- and T2-weighted imaging, diffusion-weighted imaging, and gadoxetic acid-enhanced imaging with arterial, portal, transitional, and hepatobiliary phases. The details are provided in Supplementary Methods 1 and Supplementary Table 1.

Imaging Analysis

Two abdominal radiologists (with 12 and 11 years of experience in abdominal imaging, respectively), blinded to the detailed clinical and laboratory data, independently evaluated the CT and MR images in random order. Imaging analysis was performed using a picture archiving and communication system (Centricity; GE Healthcare) with adjustment of the optimal window width and level.

https://doi.org/10.3348/kjr.2021.0407

Korean Journal of Radiology
KJR

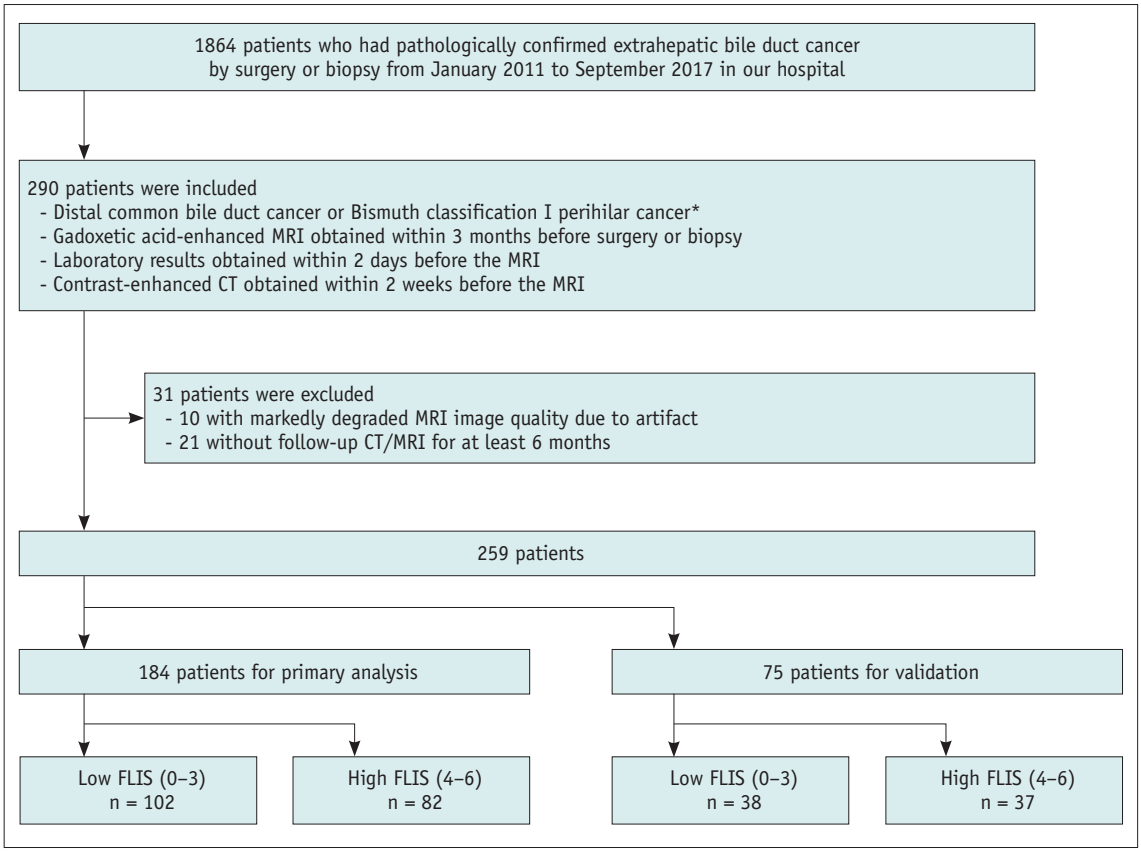

Fig. 1. Flow chart of our study. *Among perihilar cancers, only Bismuth type I was included, in which the diameter of the dilated upstream common duct could be measured. FLIS = functional liver imaging score

The following imaging parameters were evaluated on CT: 1) location of EHD cancer—perihilar or distal bile duct cancer based on the insertion site of the cystic duct [15]; 2) tumor morphology—intraductal-growing or periductal-infiltrating type [15]; 3) common duct diameter (mm), the largest diameter of the dilated upstream common duct measured on contrast-enhanced coronal image, 4) presence of biliary stent, and 5) presence of ascites.

The three FLIS parameters and the FLIS (the sum of three parameters, ranging from 0 to 6 points) were scored on the HBP image: 1) liver parenchymal enhancement quality score, a score of 0, 1, or 2 was assigned if the liver was hypo-, iso-, or hyperintense, respectively, to the right kidney, 2) biliary contrast excretion quality score—a score of 0, 1, or 2 was assigned if the liver was hypo-, iso-, or hyperintense, respectively, to the right duct, 3) portal contrast excretion quality score—a score of 0, 1, or 2 was assigned if the portal vein was hyper-, iso-, or hypointense, respectively, to the liver parenchyma (Supplementary Table 2) [13,14]. The subjective assessment of the HBP image quality using a 4-point grading scale as uninterpretable, poor (below average), fair (average), or good, and the 4-point grading scale was simply divided into acceptable (fair or good) or suboptimal (poor or uninterpretable) image qualities.

If a patient was considered to have at least one focal liver lesion requiring a differential diagnosis between microabscesses and metastasis, the reviewers scored the possibility of metastasis by assigning the following confidence level: 1, definitely a micro-abscess; 2, probably a micro-abscess; 3, probably a metastasis; and 4, definitely a metastasis. The known imaging criteria were presented to the reviewers [10,16,17], but the final decision was made based on the subjective judgment of each reviewer. Details are provided in Supplementary Methods 2. If multiple lesions were present, the largest lesion was selected. The maximal diameter of the target lesion was measured in the axial plane during any phase. The conspicuity of the target lesion in the HBP image was evaluated as poor (poor lesion conspicuity, defined as a lesion that could not be depicted).

Clinical Data and Serum Biochemical Parameter Analyses

Age, sex, etiology of liver disease, and body mass index

 https://doi.org/10.3348/kjr.2021.0407

were assessed as baseline clinical information. For the serum biochemical parameters, the serum levels of total bilirubin, aspartate transaminase (AST), alanine transaminase (ALT), alkaline phosphatase (ALP), γ-glutamyltransferase (GGT), albumin, platelet count, prothrombin time, and creatinine obtained within two days before the MRI examination were recorded.

Final Diagnosis of Focal Liver Lesions

Final diagnoses for focal liver lesions were confirmed using pathologic results from biopsy (three metastases), an increased size, and hypermetabolism on ^{18}F-fluorodeoxyglucose (FDG) positron emission tomography (PET)/CT (two metastases) or follow-up CT and/or MRI (six metastases and 34 abscesses). If the size or number of the focal liver lesions increased in the follow-up images and hypermetabolism was noted on ^{18}F-FDG PET/CT, we diagnosed it as metastasis [18,19]. If there was evidence of infection/inflammation in clinical and laboratory findings, and the lesion decreased in follow-up images, it was diagnosed as a micro-abscess [20,21].

Statistical Analyses

To evaluate the interobserver agreement in image interpretation, the κ values or weighted κ values were calculated. The consensus results of the two reviewers were used to analyze HBP image quality. All patients were classified into the low-FLIS (FLIS 0–3) or high-FLIS (FLIS 4–6) groups [13,14]. Comparisons were made using the chi-square test or Fisher's exact test for categorical variables and Student's *t* test or the Mann–Whitney U test for continuous variables. Univariable and multivariable logistic regression analyses were used to identify factors associated with the low-FLIS group. For multivariable analysis, variables with p values < 0.05, in the univariable analyses, were included in the final model. Subgroup analyses in patients with or without biliary stents were also performed. The correlations between FLIS and quantitative parameters were evaluated using Spearman or Pearson correlation coefficients. Receiver operating characteristic curve analysis was used to estimate the optimal cutoff value of the serum biochemical parameters for predicting low FLIS according to the Youden index. To validate the optimal cutoff of the serum biochemical parameters, the performance for predicting low FLIS was evaluated in the validation set. Furthermore, the performance for distinguishing hepatic metastasis from abscess was calculated for each reviewer, considering each reviewer's confidence scores of 3 or 4 as test-positive for metastasis. Comparison of the diagnostic performance for metastasis between the FLIS groups was performed using Fisher's exact test. Statistical analyses were performed using R software version 3.3.2 (The R Foundation for Statistical Computing) and SPSS version 25 (IBM Corp.). Statistical significance was set at $p < 0.05$.

RESULTS

Characteristics of the Study Groups

The baseline characteristics of all 259 patients (mean age, 68.0 ± 8.3 years; range, 43–90 years; 162 male and 97 female) are summarized in Table 1. One hundred-forty patients (54.1%) were classified into the low-FLIS group and 119 (45.9%) into the high-FLIS group. Except for the etiology of liver disease and common duct diameter, there were no significant differences between the primary and validation sets.

Table 2 shows the comparison of the clinical, imaging, and biochemical parameters between the FLIS groups in the primary analysis set. Except for the common duct diameter, there were no significant differences in clinical data and imaging findings between the two groups. The common duct diameter was larger in the low-FLIS group than in the high-FLIS group (15 mm vs. 13 mm, $p < 0.001$). The low-FLIS group showed higher serum levels of total bilirubin, AST, ALT, ALP, and GGT, and low level of albumin than the high-FLIS group ($p < 0.001$). In the low-FLIS group, 97.1% showed no biliary excretion (biliary contrast excretion quality score of 0), whereas 63.7%–79.4% showed liver parenchymal enhancement equal or higher to that of the kidney and portal vein (liver parenchymal enhancement quality score of 1 and portal vein sign quality score of 1 or 2). In the subjective assessment of the HBP image quality, 93.9% of the high-FLIS group showed acceptable image quality, whereas 47.1% of the low-FLIS group showed suboptimal image quality ($p < 0.001$).

Factors Associated with Low FLIS at the HBP of Gadoxetic Acid-Enhanced MRI

In the multivariable analysis, only the serum level of total bilirubin was an independent factor associated with low FLIS (adjusted odds ratio [OR] per 1-mg/dL increase, 1.64; 95% confidence interval [CI], 1.34–2.01; $p < 0.001$) (Table 3). In the subgroup analyses of 110 patients without biliary stents and 74 patients with biliary stents, the serum

https://doi.org/10.3348/kjr.2021.0407

Korean Journal of Radiology
KJR

Table 1. Characteristics of Study Population

	Total (n = 259)	Primary Analysis Set (n = 184)	Validation Set (n = 75)	*P*
Time of EHD cancer diagnosis		January 2014–September 2017	January 2011–December 2013	
Clinical data				
Age, years	69.0 (62.0–74.0)	68.0 (62.0–74.0)	71.0 (62.5–75.0)	0.106
Sex, male	162 (62.6)	112 (60.9)	50 (66.7)	0.464
Etiology of liver disease				0.013
Viral hepatitis B or C	23 (8.9)	22 (12.0)	1 (1.3)	
Others	236 (91.1)	162 (88.0)	74 (98.7)	
BMI	23.7 (21.9–26.0)	23.9 (21.9–26.2)	23.5 (21.8–25.1)	0.229
Imaging findings				
Tumor location				0.306
Distal bile duct	169 (65.3)	116 (63.0)	53 (70.7)	
Perihilar bile duct	90 (34.7)	68 (37.0)	22 (29.3)	
Tumor morphology				0.255
Intraductal-growing	62 (23.9)	40 (21.7)	22 (29.3)	
Periductal-infiltrating	197 (76.1)	144 (78.3)	53 (70.7)	
Common duct diameter, mm	14 (11–18)	14 (11–18)	13 (10–15)	0.037
Biliary stent insertion	94 (36.3)	74 (40.2)	20 (26.7)	0.056
Presence of ascites	21 (8.1)	13 (7.1)	8 (10.3)	0.476
Biochemical parameter				
Total bilirubin, mg/dL	2.9 (0.9–11.4)	3.3 (1.0–11.6)	2.5 (0.8–9.1)	0.401
AST, U/L	61.0 (31.0–126.0)	61.0 (32.2–127.5)	56.0 (28.5–108.0)	0.340
ALT, U/L	78.0 (27.0–197.0)	73.5 (28.0–204.5)	97.0 (24.5–168.5)	0.716
ALP, U/L	243.0 (139.0–450.0)	244.0 (141.0–446.5)	241.0 (124.5–455.0)	0.922
GGT, U/L	468.0 (200.7–1026.5)	461.5 (200.2–1057.0)	591.5 (213.5–960.5)	0.692
Albumin, g/dL	4.1 (3.7–4.4)	4.1 (3.7–4.4)	4.0 (3.7–4.3)	0.654
Platelet count*, x 10^3/μL	258.2 ± 80.5	262.4 ± 83.3	248.3 ± 73.1	0.183
Prothrombin time, INR	1.0 (0.9–1.0)	1.0 (0.9–1.1)	1.07 (0.9–1.0)	0.225
Creatinine, mg/dL	0.8 (0.7–0.9)	0.8 (0.7–1.0)	0.8 (0.7–0.9)	0.375
FLIS group				0.575
Low FLIS (FLIS 0–3)	140 (54.1)	102 (55.4)	38 (50.7)	
High FLIS (FLIS 4–6)	119 (45.9)	82 (44.6)	37 (49.3)	
Subjective HBP image quality†				0.232
Acceptable	178 (68.7)	131 (71.2)	47 (62.7)	
Suboptimal	81 (31.3)	53 (28.8)	28 (37.3)	

Unless otherwise indicated, the results are reported as numbers (%) or medians (interquartile ranges). *Data are presented as the mean ± standard deviation, †Subjective HBP image quality: acceptable image quality includes fair or good, and suboptimal image quality includes poor or uninterpretable image quality. ALP = alkaline phosphatase, ALT = alanine transaminase, AST = aspartate transaminase, BMI = body mass index, EHD = extrahepatic bile duct, FLIS = functional liver imaging score, GGT = γ-glutamyltransferase, HBP = hepatobiliary phase, INR = international normalized ratio

level of total bilirubin was also an independent factor associated with low FLIS (Supplementary Table 3), with an adjusted OR of 1.59 (95% CI, 1.23–2.05) and 1.96 (95% CI, 1.39–2.76), respectively. There was no significant association between the common duct diameter and low FLIS in both the main and subgroup analyses ($p > 0.05$).

Correlation Between the FLIS and Quantitative Parameters

The common duct diameter ($r = -0.253$; $p = 0.001$), serum levels of total bilirubin ($r = -0.780$; $p < 0.001$), AST ($r = -0.436$; $p < 0.001$), ALT ($r = -0.387$; $p < 0.001$), ALP ($r = -0.473$; $p < 0.001$), GGT ($r = -0.295$; $p < 0.001$), and creatinine ($r = -0.031$; $p = 0.001$) were negatively correlated with FLIS (Table 4). The level of albumin showed a positive correlation with FLIS ($r = 0.251$; $p = 0.001$).

Prediction of Low FLIS

Figure 2 shows the area under the receiver operating curve (AUC) of serum total bilirubin for predicting low

 https://doi.org/10.3348/kjr.2021.0407

Table 2. Comparison of the Clinical, Imaging, and Biochemical Parameters between FLIS Groups in the Primary Analysis Set

	Total (n = 184)	Low FLIS (FLIS 0–3, n = 102)	High FLIS (FLIS 4–6, n = 82)	*P*
Characteristics of study groups				
Clinical data				
Age*, years	67.5 ± 8.5	67.0 ± 8.8	68.2 ± 8.3	0.340
Sex, male	112 (60.9)	68 (66.7)	44 (53.7)	0.100
Etiology of liver disease				0.889
Viral hepatitis B or C	22 (12.0)	13 (12.8)	9 (11.0)	
Others	162 (88.0)	89 (87.3)	73 (89.0)	
BMI	24.0 (21.9–26.2)	24.2 (22.2–26.5)	23.6 (21.6–25.9)	0.416
Imaging findings				
Tumor location				0.197
Distal bile duct	116 (63.0)	69 (67.7)	47 (57.3)	
Perihilar bile duct	68 (37.0)	33 (32.4)	35 (42.7)	
Tumor morphology				0.093
Intraductal-growing	40 (21.7)	17 (16.7)	23 (28.1)	
Periductal-infiltrating	144 (78.3)	85 (83.3)	59 (72.0)	
Common duct diameter, mm	14 (11–18)	15 (12–19)	13 (10–16)	< 0.001
Biliary stent insertion	74 (40.2)	37 (36.3)	37 (45.1)	0.287
Presence of ascites	13 (7.1)	10 (9.8)	3 (3.7)	0.184
Biochemical parameter				
Total bilirubin, mg/dL	3.3 (1.0–11.7)	10.7 (5.8–14.8)	0.9 (0.5–1.4)	< 0.001
AST, U/L	58.0 (31.0–128.5)	78.0 (47.0–155.0)	31.5 (21.0–76.8)	< 0.001
ALT, U/L	74.0 (29.0–183.5)	107.0 (57.0–226.0)	33.5 (20.0–107.3)	< 0.001
ALP, U/L	232.0 (126.0–403.5)	318.0 (213.0–488.5)	124.0 (79.3–282.3)	< 0.001
GGT, U/L	461.5 (200.3–1057.0)	530.5 (327.8–1146.5)	256.5 (68.5–841.0)	< 0.001
Albumin, g/dL	4.1 (3.7–4.4)	4.0 (3.6–4.3)	4.2 (3.9–4.5)	< 0.001
Platelet count, x 10^3/μL	262.5 (200.3–306.8)	266.0 (200.5–315.5)	253.0 (202.0–301.5)	0.474
Prothrombin time, INR	1.0 (0.9–1.1)	1.0 (0.9–1.0)	1.0 (0.9–1.1)	0.078
Creatinine, mg/dL	0.8 (0.7–1.0)	0.8 (0.7–1.0)	0.8 (0.7–1.0)	0.680
Composition of the FLIS parameters				
Liver parenchymal enhancement quality score				< 0.001
0	38 (20.7)	37 (36.3)	0	
1	74 (40.2)	65 (63.7)	9 (11.0)	
2	72 (39.1)	0	73 (89.0)	
Biliary contrast excretion quality score				< 0.001
0	119 (64.7)	99 (97.1)	20 (24.4)	
1	26 (14.1)	3 (2.9)	23 (28.1)	
2	39 (21.2)	0	39 (47.6)	
Portal vein sign quality score				< 0.001
0	21 (11.4)	21 (20.6)	0	
1	62 (33.7)	62 (60.8)	0	
2	101 (54.9)	19 (18.6)	82 (100.0)	
Subjective HBP image quality†				< 0.001
Acceptable	131 (71.2)	54 (52.9)	77 (93.9)	
Suboptimal	53 (28.8)	48 (47.1)	5 (6.1)	

Unless otherwise indicated, the results are reported as numbers (%) or medians (interquartile ranges). *Data are presented as the mean ± standard deviation, †Subjective HBP image quality: acceptable image quality includes fair or good, and suboptimal image quality includes poor or uninterpretable image quality. ALP = alkaline phosphatase, ALT = alanine transaminase, AST = aspartate transaminase, BMI = body mass index, FLIS = functional liver imaging score, GGT = γ-glutamyltransferase, HBP = hepatobiliary phase, INR = international normalized ratio

https://doi.org/10.3348/kjr.2021.0407

Korean Journal of Radiology
KJR

FLIS in the primary and validation sets. The AUC of serum total bilirubin for predicting low FLIS was 0.953 (95% CI: 0.914–0.982) in the primary analysis set and 0.956 (95% CI: 0.881–0.990) in the validation set. The optimal cutoff value of 2.1 mg/dL showed a sensitivity of 95.1% (95% CI: 88.9–98.4) and a specificity of 89.0% (95% CI: 80.2–94.9) in the primary analysis set. The criterion of serum total bilirubin ≥ 2.1 mg/dL showed the sensitivity and specificity of 92.1% (95% CI: 78.6–98.3) and 83.8% (95% CI: 68.0–93.8), respectively, for predicting low FLIS in the validation set.

Table 3. Factors Associated with the Low FLIS (FLIS 0–3 Points) at Hepatobiliary Phase Imaging of Gadoxetic Acid-Enhanced MRI in the Primary Analysis Set

	Univariable Analysis		Multivariable Analysis*	
	Odds Ratio (95% CI)	*P*	Adjusted Odds Ratio (95% CI)	*P*
Clinical data				
Sex [female]	0.51 (0.25–1.05)	0.038	1.72 (0.59–0.92)	0.359
Age, years	0.98 (0.94–1.02)	0.272		
Viral hepatitis B or C [others]	1.02 (0.37–2.82)	0.975		
BMI	1.00 (0.91–1.10)	0.940		
Imaging findings				
Perihilar cancer [distal bile duct cancer]	1.50 (0.73–3.07)	0.272		
Periductal-infiltrating [intraductal-growing]	0.80 (0.35–1.83)	0.600		
Common duct diameter, mm	1.10 (1.02–1.19)	0.016	1.00 (0.88–1.13)	0.956
Biliary stent insertion [no]	0.73 (0.35–1.55)	0.417		
Presence of ascites [no]	3.55 (0.74–16.93)	0.112		
Biochemical parameter				
Total bilirubin, mg/dL	1.67 (1.37–2.03)	< 0.001	1.64 (1.34–2.01)	< 0.001
AST, U/L	1.01 (1.00–1.01)	0.016	1.00 (0.99–1.01)	0.774
ALT, U/L	1.00 (1.00–1.01)	0.005	1.00 (1.00–1.01)	0.403
ALP, U/L	1.00 (1.00–1.01)	0.002	1.00 (1.00–1.00)	0.736
GGT, U/L	1.00 (1.00–1.00)	0.017	1.00 (1.00–1.00)	0.803
Albumin, g/dL	0.31 (0.13–0.71)	0.006	0.30 (0.07–1.23)	0.095
Platelet count, x 10^3/μL	1.00 (1.00–1.01)	0.437		
Prothrombin time, INR	0.51 (0.01–26.40)	0.741		
Creatinine, mg/dL	0.82 (0.52–1.31)	0.410		

Variables in brackets are reference categories. *Logistic regression using statistically significant variables ($p < 0.05$) from the results of the univariable analyses. ALP = alkaline phosphatase, ALT = alanine transaminase, AST = aspartate transaminase, BMI = body mass index, CI = confidence interval, FLIS = functional liver imaging score, GGT = γ-glutamyltransferase, INR = international normalized ratio

Table 4. Correlation between FLIS and Quantitative Parameters

Parameter	Estimates*	Correlation Coefficient with FLIS (*r*)	*P*
Common duct diameter, mm	14.0 (11.0–18.0)	-0.253	0.001
Total bilirubin, mg/dL	3.3 (1.0–11.7)	-0.780	< 0.001
AST, U/L	58.0 (31.0–128.5)	-0.436	< 0.001
ALT, U/L	74.0 (29.0–183.5)	-0.387	< 0.001
ALP, U/L	232.0 (126.0–403.5)	-0.473	< 0.001
GGT, U/L	461.5 (200.3–1057.0)	-0.295	0.001
Albumin, g/dL	4.1 (3.7–4.4)	0.251	0.001
Platelet count, x 10^3/μL	262.4 ± 83.3	0.003	0.967
Prothrombin time, INR	1.0 (0.9–1.1)	0.135	0.078
Creatinine, mg/dL	0.8 (0.7–1.0)	-0.031	0.001

*Estimates represent median (interquartile range), except for the platelet count that represents the mean ± standard deviation.
ALP = alkaline phosphatase, ALT = alanine transaminase, AST = aspartate transaminase, FLIS = functional liver imaging score, GGT = γ-glutamyltransferase, INR = international normalized ratio

https://doi.org/10.3348/kjr.2021.0407

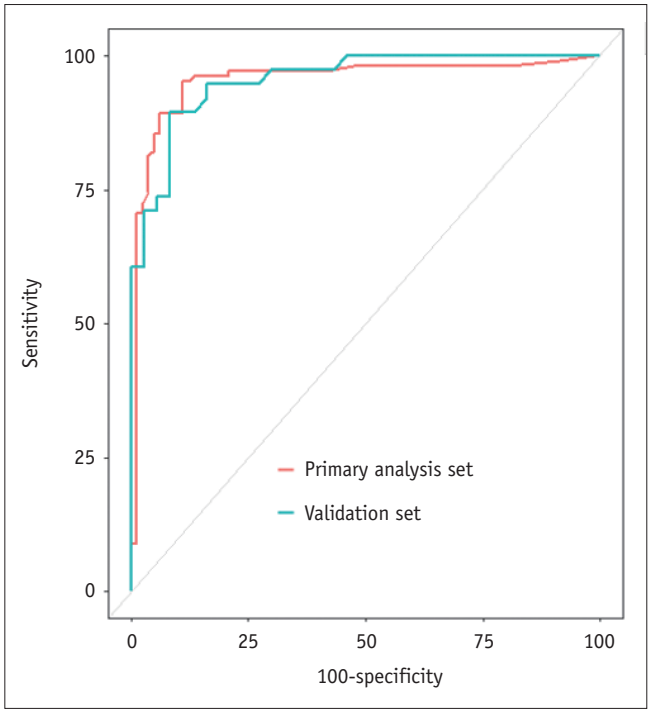

Fig. 2. The graph shows the serum level of the total bilirubin for the prediction of low functional liver imaging score in the primary analysis and validation sets. The area under the receiver operating characteristic curve was 0.953 (95% CI: 0.914–0.982) in the primary analysis set and 0.956 (95% CI: 0.881–0.990) in the validation set. The optimal cutoff value of the serum level of total bilirubin was 2.1 mg/dL with a sensitivity of 95.1% (95% CI: 88.9–98.4) and a specificity of 89.0% (95% CI: 80.2–94.9). CI = confidence interval

Characterization of Focal Liver Lesion

Among 184 patients in the primary analysis set, 45 (24.5%) had focal liver lesions, 23 (21.6%) in the high-FLIS group (Fig. 3) and 22 (28.0%) in the low-FLIS group (Table 5). The mean size of the target lesions was 1.1 ± 0.5 cm (range, 0.5–2.6 cm). The final diagnosis of the focal liver lesions included 34 abscesses and 11 metastases. In both reviewers, all lesions with poor conspicuity belonged to the low-FLIS group ($p < 0.001$) (Fig. 4). The sensitivity for diagnosing metastasis was lower in the low-FLIS group without statistical significance (50.0% vs. 100.0% in reviewer 1; 50.0% vs. 80.0% in reviewer 2) (Table 5).

The Interobserver Agreement for Imaging Assessment

The three FLIS parameters showed weighted κ values ranging from 0.84 to 0.93 (Supplementary Table 4). The 4-point grading of subjective assessment for the HBP image quality had a weighted κ of 0.78, and poor lesion conspicuity had a κ of 0.77. The distinction of liver metastasis vs. abscess for focal liver lesions showed κ of 0.77 in the high-FLIS group and κ of 0.49 in the low-FLIS group.

DISCUSSION

In patients with EHD cancer, the serum level of total bilirubin can be a predictor of the HBP image quality of MRI. Degradation of HBP images may affect the diagnostic performance for liver metastasis. The serum level of total bilirubin before MRI acquisition may help in the selection of MRI contrast agents in patients with EHD cancer, particularly when MRI is used as a problem-solving tool for the differential diagnosis between hepatic micro-abscesses and metastases.

The optimal cutoff of the serum level of total bilirubin for predicting low FLIS in our study was 2.1 mg/dL, which is similar to that (1.75 mg/dL and 2.18 mg/dL) of previous studies [3,11]. In a previous study that included patients with liver cirrhosis using gadoxetic acid-enhanced MRCP, only 40% of patients with liver cirrhosis showed sufficient image quality for visualization of the biliary tree [3]. A serum level of total bilirubin ≥ 30 μmoL/L (1.75 mg/dL) was suggested as a cutoff value for insufficient visualization of the biliary tree on HBP images [3]. Another study revealed that patients with hyperintensity of the portal vein compared to that of the liver on the HBP image ("delayed hyperintense portal vein sign") showed less biliary contrast excretion and higher levels of serum bilirubin [11]. The cutoff value of the total bilirubin for the delayed hyperintense portal vein sign was 2.18 mg/dL [11].

High bilirubin level is regarded as a relative contraindication for gadoxetic acid-enhanced MRI in some centers, with a cutoff value of bilirubin of 2.0–5.0 mg/dL [22-24]. The proposed cutoff is based on empirical data, mainly applied to patients with liver cirrhosis or chronic hepatitis, and there have been no established criteria for patients with biliary obstructions obtained through data analysis. According to the 2016 European Society of Gastrointestinal and Abdominal Radiology consensus statement, gadoxetic acid-enhanced MRI with MRCP can be obtained in the absence of liver function impairment or biliary obstruction, but there is no detailed cutoff value [25]. The cutoff value for total bilirubin from our study could be used as a criterion to assist in selecting an MR contrast agent before MRI acquisition is implemented in patients with EHD cancer.

In our study, 97.1% of the low-FLIS group showed no biliary contrast excretion, and biliary excretion seems to be

https://doi.org/10.3348/kjr.2021.0407

Korean Journal of Radiology
KJR

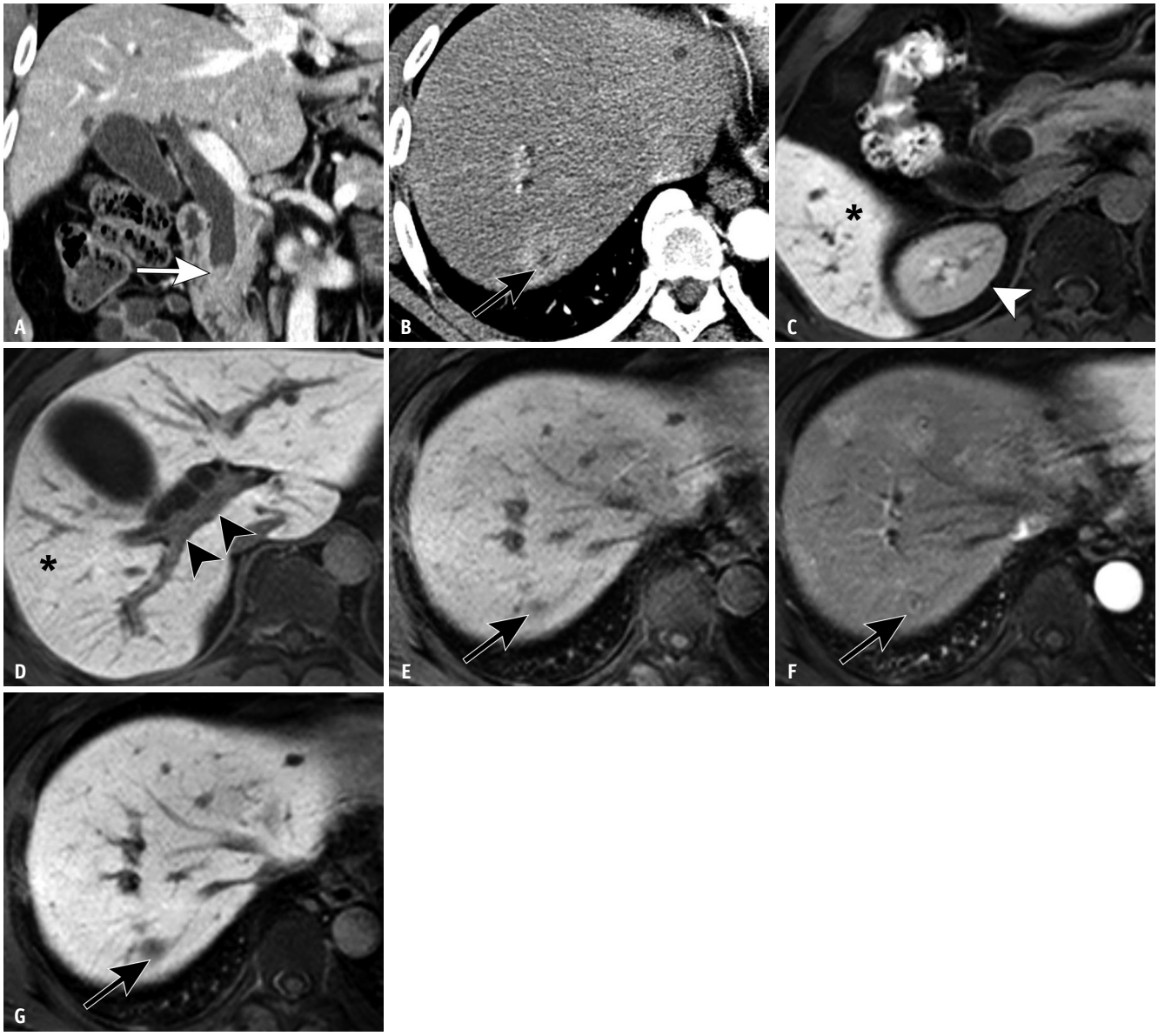

Fig. 3. A 57-year-old male with distal bile duct cancer in the high-FLIS group. The serum level of total bilirubin was 1.7 mg/dL. **A.** Contrast-enhanced CT image shows intraductal-growing distal bile duct cancer (arrow) and the dilated upstream common duct with a diameter of 15.0 mm. **B.** There is a small lesion with enhancement in periphery (arrow) in the liver segment VII. **C, D.** HBP images show hyperintensity of the liver (*, **C**) relative to the kidney (white arrowhead) (liver parenchymal enhancement quality score 2) and hypointensity of the portal vein (black arrowheads) relative to the liver (*, **D**) (portal vein sign quality score 2), but no biliary contrast excretion (biliary contrast excretion quality score 0). The FLIS is 4. **E, F.** The focal liver lesion (arrows) shows hypointensity on a precontrast T1WI **(E)** and rim enhancement on an arterial phase image **(F)**. **G.** On the HBP image, the lesion is depicted as a hypointense lesion with a fuzzy margin (arrow) that is larger than those on the T1WI. Both reviewers determined it as definitely a micro-abscess. The lesion was not seen on contrast-enhanced CT obtained after 4 months and was considered a hepatic micro-abscess (not shown). FLIS = functional liver imaging score, HBP = hepatobiliary phase, T1WI = T1-weighted image

most affected by biliary obstruction among the three HBP features of the FLIS. The mechanisms of hepatic absorption and excretion of Gd-EOB-DTPA are known as organic anion-transporting polypeptide 1B3-mediated hepatic uptake and multidrug resistance-associated protein 2 (MRP2)-mediated bile canalicular excretion [26]. Because Gd-EOB-DTPA shares the same transporters operative for bilirubin, there is reduced hepatic absorption and biliary excretion of Gd-EOB-DTPA in hyperbilirubinemia [27]. Interestingly, 52.9% of the low-FLIS group had acceptable HBP image quality, which is possibly due to preserved hepatic parenchymal enhancement apart from biliary excretion. Sun et al. [5] also reported that 67.1% of patients with bile duct cancer showed higher hepatic parenchymal enhancement on HBP

 https://doi.org/10.3348/kjr.2021.0407

Table 5. Characterization for Focal Liver Lesion

	Total	Low FLIS (FLIS 0–3)	High FLIS (FLIS 4–6)	*P*
Patients with focal liver lesion, n	45	22	23	
Final diagnosis, n (%)				0.932
Abscess	34 (75.6)	16 (72.7)	18 (78.3)	
Metastasis	11 (24.4)	6 (27.3)	5 (21.7)	
Median size of target lesion (IQR), cm	0.9 (0.7, 1.2)	0.8 (0.7, 1.0)	1.1 (0.8, 1.6)	0.092
Poor lesion conspicuity on HBP image, n (%)				
All focal liver lesions (n = 45)				
Reviewer 1	13 (28.9)	13 (59.1)	0 (0)	< 0.001
Reviewer 2	11 (24.4)	11 (50.0)	0 (0)	< 0.001
Abscess (n = 34)				
Reviewer 1	12 (35.3)	12 (75.0)	0 (0)	< 0.001
Reviewer 2	10 (29.4)	10 (62.5)	0 (0)	< 0.001
Metastasis (n = 6)				
Reviewer 1	1 (9.1)	1 (16.7)	0 (0)	> 0.99
Reviewer 2	1 (9.1)	1 (16.7)	0 (0)	> 0.99
Diagnostic performance for metastasis*				
Sensitivity (95% CI), %				
Reviewer 1	72.7 (39.0–94.0)	50.0 (11.8–88.2)	100.0 (47.8–100.0)	0.182
Reviewer 2	63.6 (30.8–89.1)	50.0 (11.8–88.2)	80.0 (28.4–99.5)	> 0.99
Specificity (95% CI), %				
Reviewer 1	97.1 (84.7–100.0)	100.0 (79.4–100.0)	94.4 (72.7–99.9)	> 0.99
Reviewer 2	91.2 (76.3–98.1)	93.8 (70.0–99.8)	88.9 (65.3–98.6)	> 0.99

*Comparison of the diagnostic performance for metastasis across the FLIS group was performed using Fisher's exact test. CI = confidence interval, FLIS = functional liver imaging score, HBP = hepatobiliary phase, IQR = interquartile range

images than on portal venous phase images, even though 86.3% did not show biliary contrast excretion. This suggests that excretion of highly cytotoxic bile salts is carefully regulated, and bile canalicular excretion is the rate-limiting step. The biliary excretion of Gd-EOB-DTPA is strictly restricted by the withdrawal of MRP2 from the canalicular membrane and shutting off of the canalicular excretion in the cholestatic liver [28,29]. Given that biliary excretion is more severely impaired than hepatic parenchymal enhancement in cholestatic liver and that hepatic parenchymal enhancement affects the evaluation of focal liver lesions rather than biliary excretion, attention should be paid to the interpretation of the results of this study using the FLIS. This index reflects both hepatic parenchymal enhancement and biliary contrast excretion.

Contrary to our expectations, the dilated common duct was not related to suboptimal HBP image quality. This could be explained by the fact that the caliber of the common duct is influenced by various confounding factors, such as an intraductal mass [30] or insertion of a biliary stent, as well as the degree of bile duct obstruction. In the subgroup analysis, total bilirubin affected the FLIS in both groups with and without biliary stents. In an animal study that conducted bilioenteric anastomosis in 11 dogs that underwent common bile duct ligation, none of the liver function assessments were normalized after 7–10 days of biliary decompression [31]. In a study of 178 patients who underwent surgery for biliary obstruction, the rate of decrease in total bilirubin followed first-order kinetics and averaged 8% per day [32]. In this study, patients with high bilirubin levels at the time of MRI acquisition, even after biliary stent insertion, showed low FLIS. It is believed that there is insufficient time to recover liver function after biliary decompression.

This study had several limitations. First, there was a selection bias due to its retrospective nature. In particular, because we only included Bismuth type I cancer among patients with perihilar cancer, our results may not be generalizable to all EHD cancer patients. This approach was inevitable when using a reliable FLIS reflecting HBP image quality irrespective of the involvement of the right or left intrahepatic bile duct. In addition, since we hypothesized

https://doi.org/10.3348/kjr.2021.0407

Korean Journal of Radiology
KJR

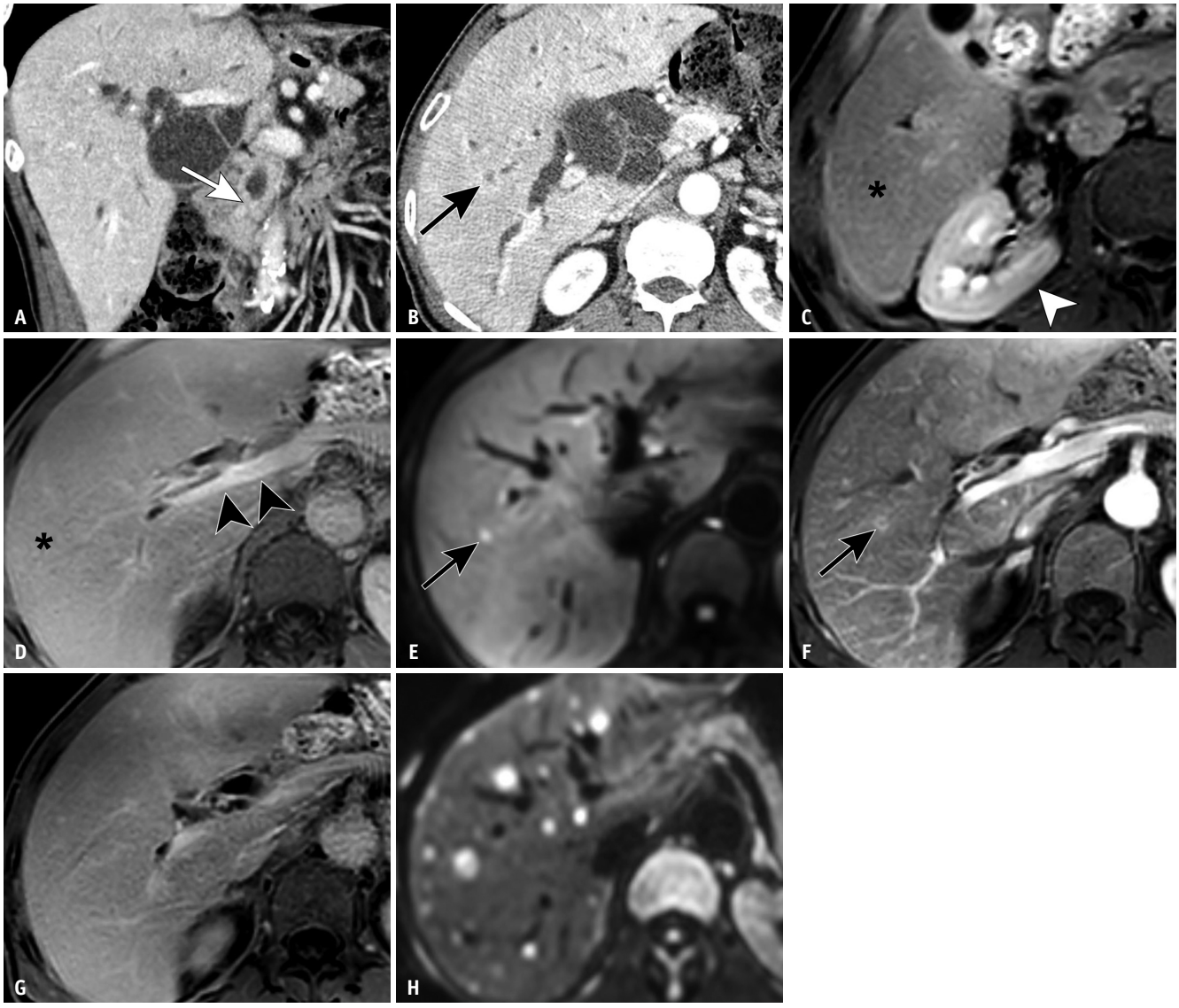

Fig. 4. A 71-year-old male with distal bile duct cancer in the low-FLIS group. The serum level of total bilirubin was 8.3 mg/dL. **A.** Contrast-enhanced CT image shows periductal-infiltrating distal bile duct cancer (arrow) and the dilated upstream common duct with a diameter of 13.6 mm. **B.** There is a small peripheral enhancing lesion (arrow) in the liver segment VIII. **C, D.** HBP images show hypointensity of the liver (∗, **C**) relative to the kidney (arrowhead) (liver parenchymal enhancement quality score 0), no biliary contrast excretion (biliary contrast excretion quality score 0), and hyperintensity of the portal vein (black arrowheads) relative to the liver (∗, **D**) (portal vein sign quality score 0). The FLIS is 0. **E, F.** The focal liver lesion (arrows) shows hyperintensity in a diffusion-weighted image **(E)** and rim enhancement on an arterial phase image **(F)**. **G.** On HBP image, the lesion does not appear to be distinguished (poor lesion conspicuity). Both reviewers were assigned as probably micro-abscess. **H.** A diffusion-weighted MR image obtained 2 months later reveals multiple hyperintense liver lesions with increased number and size, suggesting metastases. FLIS = functional liver imaging score, HBP = hepatobiliary phase

that the diameter of the dilated upstream common duct could be an important variable, we only included Bismuth type 1 cancer capable of diameter measurement. Second, this study was performed on a narrow study population focused on patients with EHD cancer. Further research in patients with diverse conditions, including other periampullary cancers, is needed. Third, a small number of patients with focal liver lesions were included in our study. Although the number of samples was small, we found that the lesion conspicuity and diagnostic performance for focal liver lesions were affected by FLIS. Fourth, MRI examinations were performed using a single 3T scanner, limiting the generalizability of our results. Lastly, we conducted temporal validation of the cutoff of the serum level of total bilirubin for predicting low FLIS using subjects in our institution. External validation using other subject groups must be performed sufficiently.

In conclusion, the serum level of total bilirubin before

 https://doi.org/10.3348/kjr.2021.0407

acquisition of gadoxetic acid-enhanced MRI may help predict suboptimal HBP image quality in patients with EHD cancer.

Supplement

The Supplement is available with this article at https://doi.org/10.3348/kjr.2021.0407.

Availability of Data and Material

The datasets generated or analyzed during the study are not publicly available due the patient's privacy but are available from the corresponding author on reasonable request.

Conflicts of Interest

The authors have no potential conflicts of interest to disclose.

Author Contributions

Conceptualization: Ji Hye Min. Data curation: Ji Hye Min, Seo-Youn Choi, Ji Eun Lee. Formal analysis: Jeong Ah Hwang, Ji Hye Min. Investigation: Jeong Ah Hwang, Ji Hye Min. Methodology: Ji Hye Min, Seong Hyun Kim. Project administration: Ji Hye Min. Resources: Jeong Ah Hwang, Ji Eun Lee, Ji Yoon Moon. Supervision: Ji Hye Min, Seong Hyun Kim. Validation: Jeong Ah Hwang, Ji Hye Min. Visualization: Jeong Ah Hwang, Ji Hye Min. Writing—original draft: Jeong Ah Hwang, Ji Hye Min. Writing—review & editing: all authors.

ORCID iDs

Jeong Ah Hwang
https://orcid.org/0000-0002-8012-995X
Ji Hye Min
https://orcid.org/0000-0002-8496-6771
Seong Hyun Kim
https://orcid.org/0000-0002-0676-2191
Seo-Youn Choi
https://orcid.org/0000-0002-2434-8779
Ji Eun Lee
https://orcid.org/0000-0002-4442-4441
Ji Yoon Moon
https://orcid.org/0000-0003-3758-2617

Funding Statement

None

REFERENCES

1. Reimer P, Schneider G, Schima W. Hepatobiliary contrast agents for contrast-enhanced MRI of the liver: properties, clinical development and applications. *Eur Radiol* 2004;14:559-578
2. Balci NC, Semelka RC. Contrast agents for MR imaging of the liver. *Radiol Clin North Am* 2005;43:887-898, viii
3. Tschirch FT, Struwe A, Petrowsky H, Kakales I, Marincek B, Weishaupt D. Contrast-enhanced MR cholangiography with Gd-EOB-DTPA in patients with liver cirrhosis: visualization of the biliary ducts in comparison with patients with normal liver parenchyma. *Eur Radiol* 2008;18:1577-1586
4. Park MJ, Kim YK, Lim S, Rhim H, Lee WJ. Hilar cholangiocarcinoma: value of adding DW imaging to gadoxetic acid-enhanced MR imaging with MR cholangiopancreatography for preoperative evaluation. *Radiology* 2014;270:768-776
5. Sun HY, Lee JM, Park HS, Yoon JH, Baek JH, Han JK, et al. Gadoxetic acid-enhanced MRI with MR cholangiography for the preoperative evaluation of bile duct cancer. *J Magn Reson Imaging* 2013;38:138-147
6. Pietryga JA, Burke LM, Marin D, Jaffe TA, Bashir MR. Respiratory motion artifact affecting hepatic arterial phase imaging with gadoxetate disodium: examination recovery with a multiple arterial phase acquisition. *Radiology* 2014;271:426-434
7. Tamada T, Ito K, Sone T, Yamamoto A, Yoshida K, Kakuba K, et al. Dynamic contrast-enhanced magnetic resonance imaging of abdominal solid organ and major vessel: comparison of enhancement effect between Gd-EOB-DTPA and Gd-DTPA. *J Magn Reson Imaging* 2009;29:636-640
8. Kaur H, Hindman NM, Al-Refaie WB, Arif-Tiwari H, Cash BD, Chernyak V, et al. ACR Appropriateness Criteria® suspected liver metastases. *J Am Coll Radiol* 2017;14:S314-S325
9. Ichikawa T, Saito K, Yoshioka N, Tanimoto A, Gokan T, Takehara Y, et al. Detection and characterization of focal liver lesions: a Japanese phase III, multicenter comparison between gadoxetic acid disodium-enhanced magnetic resonance imaging and contrast-enhanced computed tomography predominantly in patients with hepatocellular carcinoma and chronic liver disease. *Invest Radiol* 2010;45:133-141
10. Choi SY, Kim YK, Min JH, Cha DI, Jeong WK, Lee WJ. The value of gadoxetic acid-enhanced MRI for differentiation between hepatic microabscesses and metastases in patients with periampullary cancer. *Eur Radiol* 2017;27:4383-4393
11. Lee NK, Kim S, Kim GH, Heo J, Seo HI, Kim TU, et al. Significance of the "delayed hyperintense portal vein sign" in the hepatobiliary phase MRI obtained with Gd-EOB-DTPA. *J Magn Reson Imaging* 2012;36:678-685
12. Takao H, Akai H, Tajima T, Kiryu S, Watanabe Y, Imamura H, et al. MR imaging of the biliary tract with Gd-EOB-DTPA: effect of liver function on signal intensity. *Eur J Radiol* 2011;77:325-329

13. Bastati N, Beer L, Mandorfer M, Poetter-Lang S, Tamandl D, Bican Y, et al. Does the functional liver imaging score derived from gadoxetic acid-enhanced MRI predict outcomes in chronic liver disease? *Radiology* 2020;294:98-107
14. Bastati N, Wibmer A, Tamandl D, Einspieler H, Hodge JC, Poetter-Lang S, et al. Assessment of orthotopic liver transplant graft survival on gadoxetic acid-enhanced magnetic resonance imaging using qualitative and quantitative parameters. *Invest Radiol* 2016;51:728-734
15. Lee DH, Kim B, Lee ES, Kim HJ, Min JH, Lee JM, et al. Radiologic evaluation and structured reporting form for extrahepatic bile duct cancer: 2019 consensus recommendations from the Korean Society of Abdominal Radiology. *Korean J Radiol* 2021;22:41-62
16. Kim YK, Lee MW, Lee WJ, Kim SH, Rhim H, Lim JH, et al. Diagnostic accuracy and sensitivity of diffusion-weighted and of gadoxetic acid-enhanced 3-T MR imaging alone or in combination in the detection of small liver metastasis (≤ 1.5 cm in diameter). *Invest Radiol* 2012;47:159-166
17. Holzapfel K, Bruegel M, Eiber M, Ganter C, Schuster T, Heinrich P, et al. Characterization of small (≤ 10 mm) focal liver lesions: value of respiratory-triggered echo-planar diffusion-weighted MR imaging. *Eur J Radiol* 2010;76:89-95
18. Jeon SK, Lee JM, Joo I, Lee DH, Ahn SJ, Woo H, et al. Magnetic resonance with diffusion-weighted imaging improves assessment of focal liver lesions in patients with potentially resectable pancreatic cancer on CT. *Eur Radiol* 2018;28:3484-3493
19. Nino-Murcia M, Olcott EW, Jeffrey RB Jr, Lamm RL, Beaulieu CF, Jain KA. Focal liver lesions: pattern-based classification scheme for enhancement at arterial phase CT. *Radiology* 2000;215:746-751
20. Méndez RJ, Schiebler ML, Outwater EK, Kressel HY. Hepatic abscesses: MR imaging findings. *Radiology* 1994;190:431-436
21. Bächler P, Baladron MJ, Menias C, Beddings I, Loch R, Zalaquett E, et al. Multimodality imaging of liver infections: differential diagnosis and potential pitfall. *Radiographics* 2016;36:1001-1023
22. Merkle EM, Zech CJ, Bartolozzi C, Bashir MR, Ba-Ssalamah A, Huppertz A, et al. Consensus report from the 7th international forum for liver magnetic resonance imaging. *Eur Radiol* 2016;26:674-682
23. Bashir MR, Gupta RT, Davenport MS, Allen BC, Jaffe TA, Ho LM, et al. Hepatocellular carcinoma in a North American population: does hepatobiliary MR imaging with Gd-EOB-DTPA improve sensitivity and confidence for diagnosis? *J Magn Reson Imaging* 2013;37:398-406
24. Cruite I, Schroeder M, Merkle EM, Sirlin CB. Gadoxetate disodium-enhanced MRI of the liver: part 2, protocol optimization and lesion appearance in the cirrhotic liver. *AJR Am J Roentgenol* 2010;195:29-41
25. Neri E, Bali MA, Ba-Ssalamah A, Boraschi P, Brancatelli G, Alves FC, et al. ESGAR consensus statement on liver MR imaging and clinical use of liver-specific contrast agents. *Eur Radiol* 2016;26:921-931
26. Ricke J, Seidensticker M. Molecular imaging and liver function assessment by hepatobiliary MRI. *J Hepatol* 2016;65:1081-1082
27. Ni Y, Lukito G, Marchal G, Cresens E, Yu J, Petré C, et al. Potential role of bile duct collaterals in the recovery of the biliary obstruction: experimental study in rats using microcholangiography, histology, serology and magnetic resonance imaging. *Hepatology* 1994;20:1557-1566
28. Stanca C, Jung D, Meier PJ, Kullak-Ublick GA. Hepatocellular transport proteins and their role in liver disease. *World J Gastroenterol* 2001;7:157-169
29. Elferink RP, Paulusma CC. MRP2 in cholestasis: putting down the anchor. *J Hepatol* 2015;63:1309-1310
30. Aslam A, Wasnik AP, Shi J, Sahai V, Mendiratta-Lala M. Intraductal papillary neoplasm of the bile duct (IPNB): CT and MRI appearance with radiology-pathology correlation. *Clin Imaging* 2020;66:10-17
31. Fraser IA, Shaffer P, Tuttle SV, Lessler MA, Ellison EC, Carey LC. Hepatic recovery after biliary decompression of experimental obstructive jaundice. *Am J Surg* 1989;158:423-427
32. Pellegrini CA, Thomas MJ, Way LW. Bilirubin and alkaline phosphatase values before and after surgery for biliary obstruction. *Am J Surg* 1982;143:67-73

 https://doi.org/10.3348/kjr.2021.0407